

Sub-arcsec resolution infrared images of the star forming region G 35.20-1.74*

Paolo Persi¹, Marcello Felli², Pierre O. Lagage³, Miguel Roth⁴, and Leonardo Testi⁵

¹ Istituto Astrofisica Spaziale, CNR CP.67, I-00044 Frascati, Italy

² Osservatorio Astrofisico di Arcetri, Largo E. Fermi 5, I-50125 Firenze, Italy

³ CEA/DSM/DAPNIA, Service d'Astrophysique(URA 2052 du CNRS), CE Saclay, F-91191 Gif-sur-Yvette, France

⁴ Las Campanas Observatory, Carnegie Institution of Washington, Casilla 601, La Serena, Chile

⁵ Dipartimento di Astronomia e Scienza dello Spazio, Largo E. Fermi 5, I-50125 Firenze, Italy

Received 4 March 1997 / Accepted 29 May 1997

Abstract. We present J(1.25 μm), H(1.65 μm), K(2.2 μm), H₂(2.125 μm) and 11.2 μm infrared images at sub-arcsec resolution of an area centered around the star forming region G 35.20-1.74. In J, H and K a cluster of early type stellar sources with infrared excess clearly stands out with respect to the background distribution and is associated with a diffuse K emission around an UC HII region (which is the brightest source at K). No H₂ emission is detected in narrow-band images at 2.125 μm .

At 11.2 μm six components are detected. The brightest one (MIR3) is extended and coincides with the UC HII region. The source with steepest IR spectrum and the largest infrared excess (MIR1) is associated with an H₂O maser and a near IR source detected only at K. It is separated from the IR cluster and at a distance of 20'' from the UC HII region. The IR emission comes from a local young stellar object (YSO) associated with the maser. The lack of radio continuum emission from MIR1 confirms that H₂O masers can trace the youngest evolutionary stages of massive YSOs, much before the appearance of a radio UC HII region and shows that star formation is not limited to the IR cluster (where most probably it has already come to an end) but is still taking place in other parts of the molecular cloud. Of the other 11.2 μm sources, three (MIR2, MIR4 and MIR5) present IR excesses and are similar to MIR1, while MIR6 appears to be a reddened early-type star.

The morphology of the entire star forming complex, taking into account also molecular and sub-mm observations, is indicative of different and independent episodes of star formation taking place in the same molecular cloud.

Key words: ISM: HII region; jets and outflows; molecules; G35.20 1.74 – stars: formation – infrared: stars

Send offprint requests to: P. Persi

* Based on observations obtained at CFHT and Las Campanas Observatories

1. Introduction

Radio ultra-compact HII regions (UC HII), H₂O masers and infrared (IR) sources with IR excess are the trademarks of star forming regions (SFRs). However, although they are all present in the same SFR, they may not be necessarily physically related to the *same* YSO. In fact, new indications from high resolution observations suggest that each of them may represent a *different and independent* YSO and that the possible associations between them, that occur in some cases, may simply reflect the fact that each type of emission may overlap in time with the others during the evolution of a YSO.

In particular, there is now increasing evidence, coming from the comparison of arcsec resolution radio and IR observations, that the conditions required to produce strong water maser emission occur in an evolutionary phase prior to the formation of an UC HII region. In fact, when observed in the radio at high resolution and sensitivity, many masers do not show any associated continuum source or are not directly related to UC (or more extended) HII regions also present in the same area (Tofani et al. 1995, Hunter et al. 1995, Palla et al. 1995, Felli et al. 1997, Persi et al. 1996, Hofner & Churchwell, 1996, Codella et al. 1997). Similarly, submillimeter continuum observations in the vicinity of H₂O masers (Jenness et al. 1995) also show that the majority of the sub-mm sources detected are directly related to the water maser and not to the UC HII regions. This further supports the association of H₂O masers with the earliest manifestation of a YSO, i.e. when it is detectable only as a moderately warm (25 - 50 K) and luminous dust core. Finally, molecular observations in high density tracers like CS, NH₃, CH₃CN confirm that the masers are found associated with compact and dense molecular blobs, not necessarily coincident with UC HII regions (Turner & Welch, 1984, Wink et al. , 1994, Cesaroni et al. 1994, Codella et al. 1997).

Forster & Caswell (1989), observing with VLA a sample of OH and H₂O masers associated with 74 star forming regions

at arcsec resolution, found that the maser sources occur near a common center but in physically distinct zones and that there was *no* evidence that the centers were coincident with the continuum peaks. Testi et al. (1994), imaging in the near-IR a sub-sample of these sources, discovered very faint K sources (all with a strong IR excess) within few arcseconds from the H₂O masers. They concluded that the maser activity is characteristic of the youngest phases of the life of a YSO and that the near IR emission comes from an associated YSO, detectable only in the IR and not in the radio continuum. The IR excess can be due to a hot circumstellar dust envelope around the YSO, free-free and bound-free emission from ionized gas or photospheric stellar radiation (either direct or reflected). In any case, the close association of an IR source with the H₂O maser is the best proof of a close-by YSO responsible for its excitation.

Near IR emission in SFRs may be also associated with diffuse HII regions. In this case it is usually extended and comes from the contribution of the ionized gas, with possible weaker contributions from reflected starlight and from the near IR tail of the dust emission (Natta & Panagia 1976).

In summary, the fact that UC HII regions, OH and H₂O masers and near IR sources are found in the same region may merely reflect the formation of a stellar cluster inside a molecular cloud and does not imply an unique YSO responsible for all the emissions. However, in order to establish the true associations between the different types of emission as well as their occurrence during the lifetime of a YSO, high resolution radio and near IR observations are required. Mid infrared observations with similar resolutions are also essential to better define the spectral energy distribution (SED) of each source.

To achieve this goal we have undertaken a project of near and mid-infrared images at arcsec resolution of a selected sample of H₂O masers from the list of Forster & Caswell (1989). In the present work, the results relative to the near and mid-IR images obtained with similar sub-arcsec resolution of the SFR known as G 35.20-1.74 are discussed. This nomenclature usually refers to the UC HII region; we shall use it in a broader sense referring to the entire SFR-molecular cloud complex. We shall also compare our observations with radio continuum, molecular and sub-mm observations taken from the literature.

G 35.20-1.74 is the most compact (angular diameter $\simeq 4''$, Woodward et al. 1985) of the W48 cluster of HII regions (W48A in the nomenclature of Onello et al. 1994). When observed with even higher resolution ($\simeq 1''$) the radio continuum morphology is that of a cometary UC HII region (Wood & Churchwell 1989, hereafter WC). OH and H₂O masers, discovered from this source with single dish observations (Turner 1979; Genzel & Downes 1977) were found to be located at angular separations $\geq 20''$ to the N-W of the UC HII region (Forster & Caswell 1989, Hofner & Churchwell 1996). In the following we shall use the positions of the two H₂O masers reported by Hofner & Churchwell (only one maser was reported by Forster & Caswell), obtained with a resolution a factor 3 better than that of Forster & Caswell, and call them HC1 ($\alpha(1950) = 18^h 59^m 13.091^s$, $\delta(1950) = 01^\circ 09' 11.15''$) and HC2 ($\alpha(1950) = 18^h 59^m 10.721^s$, $\delta(1950) = 01^\circ 09' 15.27''$). Previous infrared

studies (Dyck & Simon 1977, Zeilik & Lada 1978, Moorwood & Salinari 1981), detected only a single bright source with a luminosity between 1 and 33 μm of $\simeq 10^5 L_\odot$. Given the large diaphragms used ($\simeq 20''$) it was not possible to discriminate between the UC HII region and the maser. More recently, a new near-IR image of the region, besides revealing the structure of the diffuse gas around the UC HII region and of the UC HII region itself, also showed a weak source detectable only at K (13.1 mag) close to the HC1 maser (Testi et al. 1994). The UC HII region and the masers are located close to an extended molecular cloud. Vallée & MacLeod (1990) estimated a total mass for the molecular cloud of 1500 M_\odot from CO observations. The presence of higher density molecular blobs within the molecular cloud at the position of HC1 is suggested by observations in other molecules, such as CS(J=1-0) and NH₃ (Anglada et al. (1996), Churchwell et al. 1990, Churchwell et al. 1992), even though in all cases the resolution is not adequate to separate independent components on the scale size of the UC HII region-HC1 separation. The visual extinction towards the complex has been derived from CO observations (Vallée & MacLeod 1990) and from the Br α /Br γ ratio (Woodward et al. 1985); both determinations give $A_V \geq 23$. A distance between 3.2-3.4 kpc was assigned by Bridle & Kesteven (1972); in the following we shall use the more recently adopted value of 3.1 kpc (see e.g. Churchwell et al. 1990).

2. Observations and results

2.1. Near-infrared images

The broad and narrow-band near-IR images were made on the night of 16 June 1994 with the Las Campanas Observatory Near-Infrared Camera (Persson et al. 1992) on the 2.5m DuPont telescope under sub-arcsec seeing conditions. The camera has a NICMOS3 256 \times 256 HgCdTe detector and the scale was 0.35 $''/\text{pixel}$.

The narrow-band filters are centered at $\lambda_o = 2.125 \mu\text{m}$ ($\Delta\lambda = 0.024 \mu\text{m}$), which includes the H₂ v=1-0 S(1) line, and at $\lambda_o = 2.20 \mu\text{m}$ ($\Delta\lambda = 0.11 \mu\text{m}$) for measuring the neighboring continuum.

For each filter, five images were taken in the immediate vicinity of the region, some of them also including the program object in different positions to increase the on-source integration time and at the same time, increasing the covered area. The individual frames were reduced by sky subtracting and flat fielding using the median of all images. Flux calibration was done by observing standards from the lists of Elias et al. (1982), of UKIRT (Users Manual), and of Las Campanas Observatory. Stellar photometry was performed with DAOPHOT (Stetson 1987) within IRAF, with an aperture of 3 $''$. Astrometry of the sources was obtained using the digitized Palomar Sky Survey. The limiting magnitudes are 19.6, 18.7 and 17.0 at J, H and K, respectively

J(1.25 μm), H(1.65 μm), K (2.2 μm) and H₂(2.125 μm) mosaics of dimensions 104 \times 104 square arcsec are shown in Fig.1

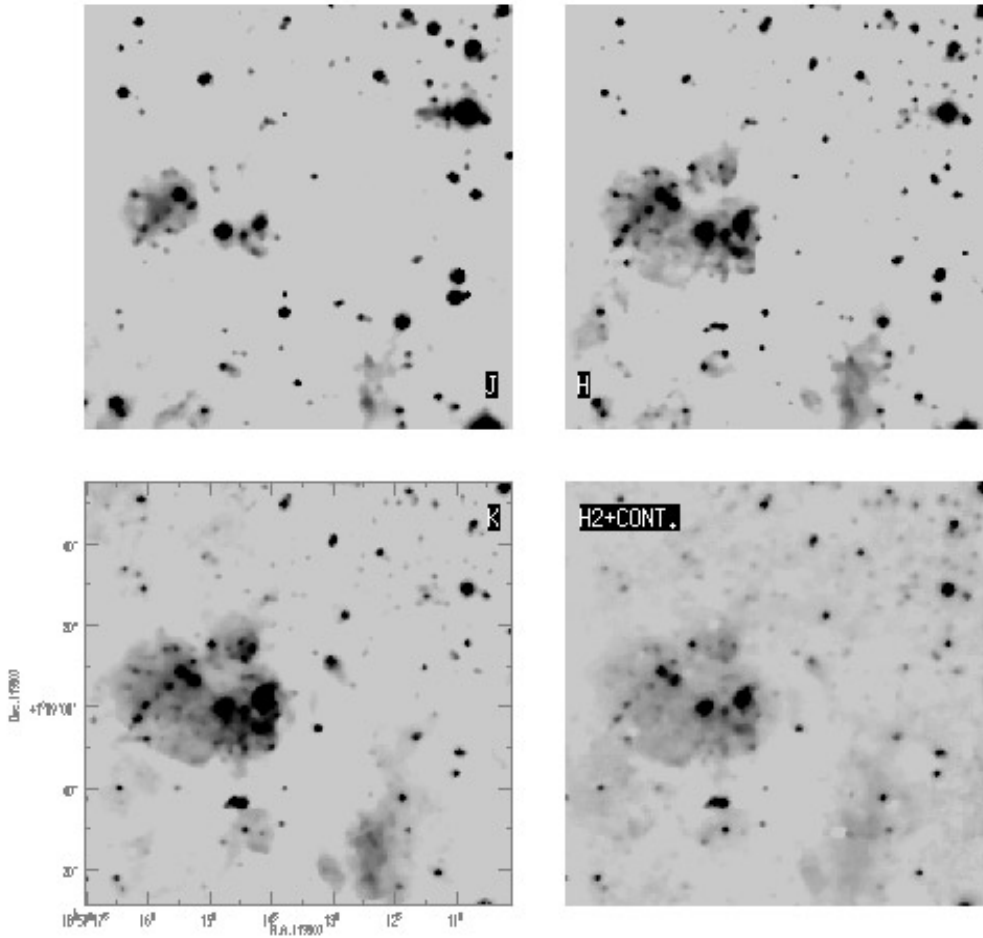


Fig. 1. Mosaics (each of five frames) covering 104×104 square arcsec in the J , H , K and H_2 of G 35.20-1.74. North is at top, east to the left.

The images, especially in K , are characterized by the presence of an extended IR nebula (size $\sim 40''$) at the west border of which is located a bright source identified with the UC HII region. A smaller IR diffuse nebulosity is observed in the SW part of the image. An infrared source with a localized nebulosity is seen at the position of HC1 and is detected only at K . A weaker near IR source maybe associated with HC2. Finally, the comparison between the H_2 image and the adjacent continuum does not show any molecular hydrogen emission above the noise level of 10^{-15} ergs cm^{-2} s^{-1} . Consequently, no image of the H_2 minus continuum is shown.

2.2. Mid-infrared image

The narrow-band image at $11.2 \mu\text{m}$ ($\Delta\lambda = 0.44 \mu\text{m}$) was obtained during an observing run on July 1996 at the Canadian-France-Hawaii-Telescope (CFHT) with the mid-IR camera CAMIRAS, and is shown in Fig.2. CAMIRAS was developed at the Service d'Astrophysique at Saclay (Lagage et al. 1992) and operates with a 192×128 Si:Ga/DVR detector array, manufactured by the Laboratoire Infrarouge (LIR) at Grenoble. We used a scale of $0.31''/\text{pix}$, and the measured point-spread function was of $\simeq 0.9$ - $1.0''$. The sky and telescope emissions were subtracted using chopping and nodding technique. The absolute

calibration of the image was obtained observing the standard stars γ Aql and η Sgr at approximately the same air mass. The astrometry of the MIR image was made comparing it with the K image.

We detected six MIR sources and a diffuse nebulosity east of the UC HII region, with embedded at least three of the MIR sources. The bright source MIR3 has an extension of $\simeq 8''$ and coincides with the brightest source seen in K and with the UC HII region. The positions and the flux densities of the sources are given in Table I. The statistical photometric errors are also reported in Table I for the $11.2 \mu\text{m}$ flux densities.

We note that IRAS18592+0108, which is usually associated with the UC HII region, is located more than $10''$ to the south of it. The IRAS $12 \mu\text{m}$ flux (114 Jy) is about a factor 4 greater than that of the $11.2 \mu\text{m}$ UC HII region (and also of the entire flux density present in our $11.2 \mu\text{m}$ map). Consequently, the IRAS fluxes (together with those at longer wavelengths) are representative of the entire SFR and should not be directly associated with the UC HII region. The difference in fluxes suggests that the contribution to the FIR emission from an extended dust cloud is much larger than that of the UC HII region.

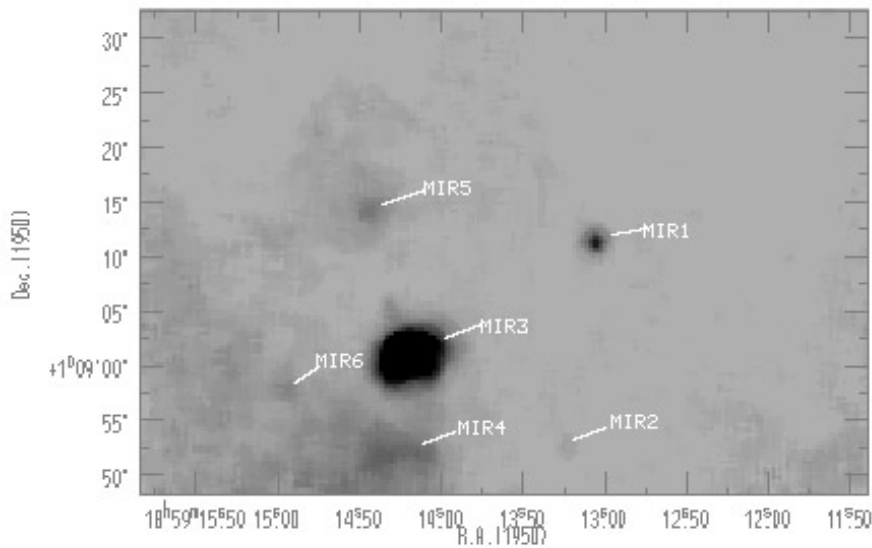


Fig. 2. 11.2 μm image of G 35.20-1.74. The image has dimension 59.5×39.7 square arcsec. The positions of the 6 MIR sources are indicated.

Table 1. Coordinates and IR photometry of the sources associated with the molecular cloud.

Source #	R.A.(1950) h m s	Dec.(1950) o ' "	J (mag.)	H (mag.)	K (mag.)	F(11.2) (Jy)	Note
1	18 59 10.89	19 16.0	17.4	15.0	13.1		HC2
2	18 59 12.38	18 48.4		17.5	15.3		
3	18 59 12.38	18 15.8	17.1	16.3	14.6		
4	18 59 12.39	19 45.2		17.7	15.0		
5	18 59 12.56	19 36.8		17.5	15.3		
6	18 59 13.06	19 11.2			12.8	1.6(.10)	MIR1 HC1
7	18 59 13.24	18 54.4	19.3	15.5	12.4	0.2(.10)	MIR2
8	18 59 13.97	18 49.5		15.9	13.6		
9	18 59 14.08	19 26.3	16.9	15.4	14.3		e
10	18 59 14.10	18 27.2		17.4	14.8		
11	18 59 14.13	19 01.6	14.3 ^a	11.9 ^a	9.8 ^a	27.8(2.0)	MIR3,UC HII
12	18 59 14.25	18 54.3	17.2	15.5	13.6	1.1(.20)	MIR4
13	18 59 14.28	19 14.4		16.0	13.3	0.8(.10)	MIR5
14	18 59 14.31	19 06.7		17.5	14.4		
15	18 59 14.41	19 11.7		16.2	13.8		
16	18 59 14.42	18 35.1		14.3	11.4		
17	18 59 14.42	18 58.0	16.9	14.9	13.7		e
18	18 59 14.45	18 50.8		16.6	14.5		
19	18 59 14.48	19 15.3	17.8	15.5	13.7		
20	18 59 14.67	19 13.0		17.1	14.5		
21	18 59 14.74	18 59.1	13.9	11.7	10.2	0.3(.10)	MIR6,e
22	18 59 14.85	19 31.3		17.5	15.1		
23	18 59 14.92	19 35.1		17.6	15.1		
24	18 59 14.95	19 14.9	17.6	14.7	12.7		
25	18 59 15.20	19 06.2	16.7	14.3	12.6		
26	18 59 15.44	19 08.1	14.9	13.2	12.1		e
27	18 59 15.46	18 58.7	18.3	16.5	14.9		
28	18 59 15.54	19 13.4	17.3	15.6	14.1		
29	18 59 15.64	19 04.3	17.7	15.6	13.9		
30	18 59 15.82	19 02.0	17.5	16.2	15.2		e
31	18 59 16.00	18 59.5	17.2	15.1	13.5		
32	18 59 16.10	18 55.9	17.4	15.1	13.3		
33	18 59 16.16	19 08.0	17.2	15.4	14.3		e

^a) photometry with 14'' aperture.

Notes: e \equiv reddened early-type stars; MIR \equiv mid-IR sources

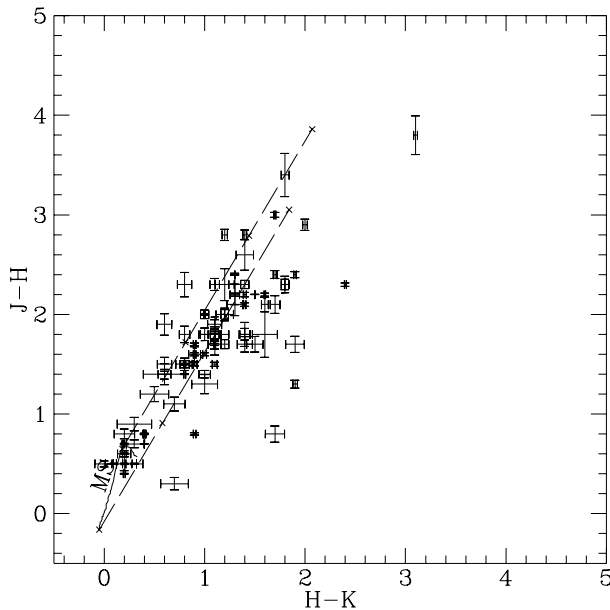


Fig. 3. $J - H$ vs $H - K$ diagram of the sources detected in the three colors towards G 35.20-1.74. The continuous line marks the locus of the main sequence stars (MS), while the two parallel dashed lines follow the reddening vector for early and late type stars. The cross on each point represents the error on the color derived from the photometric error.

3. Discussion

3.1. $J-H$ vs $H-K$ diagram

In an area of approximately 2×2 square arcmin centered around the OH/H₂O masers, we have detected 178 sources at K, of which 121 have been also observed in J and H filters. From their measured magnitudes, we have constructed the $J - H$ versus $H - K$ diagram reported in Fig.3.

According to the location of the sources in this plot, we can distinguish field stars from sources belonging to the stellar cluster. In fact, foreground and background stars are located along the main-sequence line (MS in Fig.3) or along the reddening line, while candidate young stellar objects, with an IR excess due to a circumstellar dust envelope, are those to the right of the reddening line. However, we note that as much as 50% of possible T Tauri stars may still be located on the strip of the reddened main sequence (Aspin & Barsony 1994). In addition, several objects have colors of reddened early type stars with $A_V = 15-25$, in agreement with the derived visual extinction. Therefore, the analysis of the color-color diagram, suggests the presence in G 35.20-1.74 of a conspicuous number of YSOs and early-type stars possibly related to the same star-forming region.

3.2. Infrared cluster and the K-luminosity function

The other tool to study the physical association of IR sources belonging to the same complex is to examine their spatial distribution. This is reported in Fig.4.

For comparison, in this figure we show the spatial distributions of all the sources detected in K, of those detected only in K, of those with infrared excess, and those without IR excess as derived from the two colors plot of Fig.3. We have included in the IR excess sources also those with $H - K \geq 2$ but not detected in J. In Fig.4 the positions of the UC HII region (open triangle), of the OH (filled triangle) and of the two H₂O (filled square) masers are also illustrated. As shown in the figure, most of the sources with IR excess are concentrated in an area of approximately $20''$ in radius around the position of the UC HII region and inside the extended IR nebula, while the objects classified as field stars (no IR excess) lie mainly in the NW part of the region. Therefore, Fig.4 shows the presence of a young stellar cluster in G 35.20-1.74, composed by at least of 21 embedded objects with circumstellar dust, and other six reddened early type-stars, all within the boundary of the diffuse K emission. Figure 4 also shows that the extinction towards the stellar cluster is larger than in the surrounding regions, since in this area (as well as in that of the molecular cloud, see Sect.3.6) the density of background stars is lower. Similar embedded young stellar clusters have been found associated to others star forming complexes such as M17 (Lada et al. 1991), NGC 3567 (Persi et al. 1994) and LkH α 101 (Aspin & Barsony 1994). Table I gives the position and the near-IR photometry of the objects with IR excess and with $H - K \geq 2$ but no detection in J found in G 35.20-1.74. In the same table two additional sources are given: that associated with HC1 (and MIR1), which is detected only at K, and that associated with HC2.

To study the nature of these sources, we have compared in Fig.5, the K magnitude distribution of all sources (K-luminosity function (KLF)) with that of the sources with and without IR excess, and sources detected only in K.

The total KLF peaks at $K=15.5$ mag, while the histogram of the cluster members (IR excess stars), is completely different from the other objects, and peaks at $K=13.5$ mag ($M_K \simeq -1.4$ if $A_V=23$) suggesting that the young embedded cluster has a high percentage of bright early type stars (spectral types between B2-B3 if $A_V=23$).

3.3. Infrared energy distribution

All the mid-IR sources have been detected at K. MIR1 and MIR3 correspond to the H₂O maser HC1 and the UC HII region respectively. These sources will be discussed separately in the next sections. Combining the near-IR and the $11.2 \mu\text{m}$ flux densities, we have derived their infrared energy distribution illustrated in Fig.6.

The sources MIR2, 4 and 5 show a very steep energy distribution with a clear IR excess, also evident in the two colors plot of Fig.3, while the source MIR6 has a spectrum typical of a reddened early-type stars without IR excess. In addition MIR4, 5 are located within the diffuse nebulosity observed in the near and mid-infrared, and belong to the observed young embedded cluster discussed in Sect.3. 2.

The spectral slope between 2.2 and $11.2 \mu\text{m}$, defined as

$$\alpha = \frac{d \text{Log}(\nu F_\nu)}{d \text{Log} \nu}$$

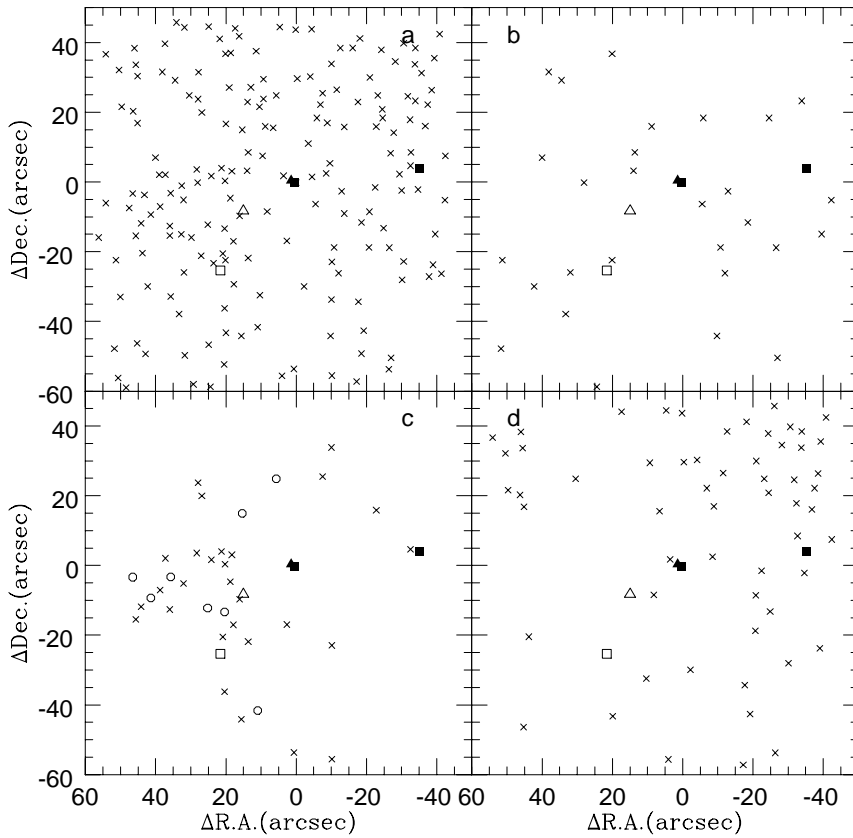


Fig. 4a–d. Spatial distribution of the near-IR sources found in G 35.20-1.74: **a** all sources detected at K, **b** sources detected only at K, **c** sources with IR excess or $H - K \geq 2$, **d** sources without IR excess. Open circles indicate sources classified as early type stars. An open triangle shows the position of the UC HII region, while filled triangles and squares show the positions of the HC1 and HC2 OH and H₂O masers, respectively. The open square marks the position of the IRAS source. The (0,0) offset corresponds to the position of the maser HC1 \equiv MIR1.

is often used to classify the evolutionary state of a YSO (Lada 1987; Andr e & Montmerle 1994). Negative values of α are those of class I sources and represent the earliest stages of evolution, when the protostar is still deeply surrounded by a thick dust envelope, class II objects are those with $0 < \alpha < 2$ and represent pre-main sequence stars surrounded by an optically thick disk, and class III objects ($\alpha > 2$) are the more evolved and surrounded by an optically thin disk.

In our case MIR1, MIR3, MIR4 and MIR5 have α equal to -2.5, -2.6, -2.8 and -2.4, respectively, and can be classified as extreme class I objects. MIR2, with $\alpha = -1.0$ can still be considered as a class I object, while MIR6 with $\alpha = 0.0$ is a transition object between class I and class II.

3.4. The UC HII region

The morphology of the UC HII region is best described by the 2 and 6 cm radio continuum maps of WC. The structure is classified as "cometary", but the possibility of a blister type configuration has also been considered. This last hypothesis was reputed less appealing because the bright sharp edge of the radio emission is on the NE side, while the molecular cloud (see Sect.3.6 and Fig.9) extends to the SW of the UC HII region. However, none of the available molecular maps has the required resolution (2-3'') necessary to study the molecular gas distribution (in high density tracers) on the NE side of the bright radio continuum edge, so the point cannot be settled for the moment.

Using the original (u,v) data of the VLA observations of WC, larger field maps at 2 and 6 cm were made. The overlay on the K image of the 6 cm map is shown in Fig.7. This shows that there is a very good agreement between the K and radio emission. A similar comparison with the 11.2 μm image also shows a very good coincidence between the two emissions.

The UC HII region radio continuum flux density at 5 GHz is 1.93 Jy. In the following we shall compare this value with the fluxes measured in the NIR and MIR, with the provision that this is the most difficult part of the spectrum, since the photosphere of an early type star, the ionized gas and the dust can give comparable contributions at K (see e.g the models of Natta & Panagia 1976). The expected K emission from the ionized gas (with no correction for extinction) can be obtained from the relation $F_K(\text{Jy}) = 0.26 S_{5\text{GHz}}(\text{Jy})$ (Howard et al. 1994), and is 500 mJy. The measured flux density at K in a 14'' diaphragm is (see Table 1) 81 mJy. For $A_V = 23$, the expected K emission becomes 75 mJy. As far as the photospheric stellar contribution is concerned, the spectral type of the early type star ionizing the UC HII region is (from radio data) O7.5 (WC). Using the stellar parameters tabulated by Panagia (1973) for ZAMS stars, the expected stellar photosphere contribution, after correction for extinction, is 23 mJy. Given the uncertainties, the sum of the two is in very good agreement with the observed value and shows that the dominant contribution comes from the free-free and free-bound emission of the ionized gas. The agreement between the extended radio and K emission also favors gas emis-

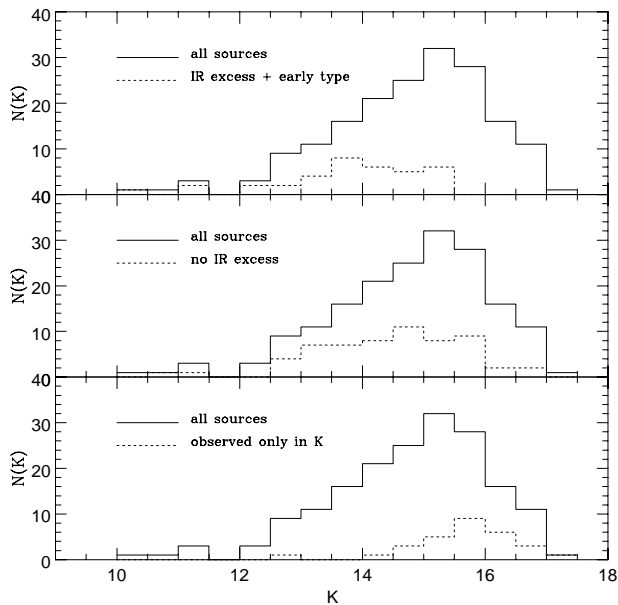


Fig. 5. Upper panel: Observed KLF for all sources detected in our K image, compared with that of sources with IR excess. Central panel: KLF of all sources compared with no IR sources. Lower panel: KLF of the sources detected only in K compared with all sources.

sion rather than stellar emission. There does not seem to be the need of reflected emission and intrinsic dust emission should be negligible, excluding the presence of very hot dust within the UC HII region.

At J the comparison changes in favor of a larger stellar contribution, since the expected stellar emission is 1.8 mJy, to be compared with an observed value (in a $14''$ aperture) of 2 mJy.

At $11.2 \mu\text{m}$, the situation is reversed, the ionized gas and the star contribute at most few percent to the observed 27.8 Jy. The emission must come from warm dust. In fact, an increase of at least an order of magnitude from K to $11.2 \mu\text{m}$ due to dust emission is expected from model calculations (Natta & Panagia 1976). The good agreement between $11.2 \mu\text{m}$ and radio maps shows that dust is well mixed with the ionized gas inside the UC HII region. However, it is difficult with only the $11.2 \mu\text{m}$ flux to estimate the temperature of the dust within the UC HII region. In fact, given the already mentioned difference between the $12 \mu\text{m}$ IRAS flux and the $11.2 \mu\text{m}$ flux, no extrapolation to longer wavelengths using IRAS data is feasible for the UC HII region.

WC noticed that the total luminosity derived from the integral of the IRAS fluxes is larger ($\text{Log}(L_{\text{IRAS}}/L_{\odot}) = 5.45$) than that derived from the spectral type of the ionizing star, estimated from the radio continuum (for an O7.5 $\text{Log}(L/L_{\odot}) = 4.92$). This effect was found to be consistently present over the large sample of UC HII regions examined by WC. Two possible solutions were examined by WC: 1) strong dust absorption of uv photons inside the UC HII region, which underestimates the spectral type of the exciting star and 2) presence of a stellar cluster with a large population of luminous, but non-ionizing stars, which

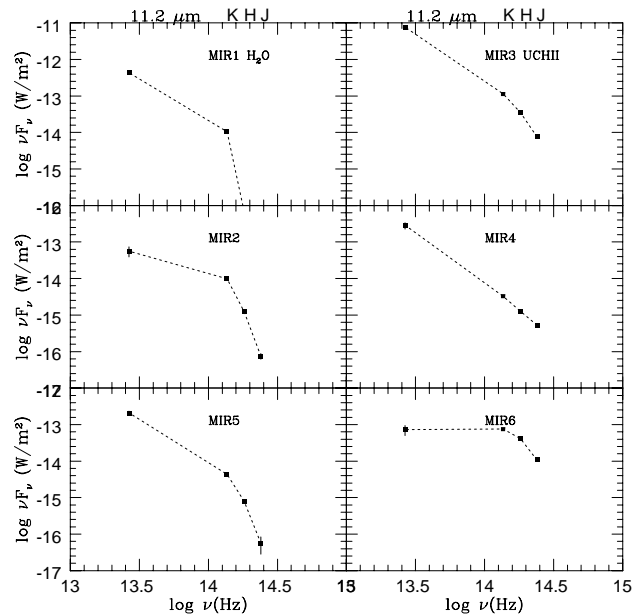


Fig. 6. Infrared energy distribution of the six sources in G 35.20 -1.7

may substantially contribute to the total luminosity. In view of our new observations we favor the second hypothesis. In fact, for the densities present in the UC HII region (the peak density is $8.6 \cdot 10^4 \text{ cm}^{-3}$), dust absorption of uv photons should be small (Felli, 1979), while a cluster of luminous stars is found in the NIR observations.

3.5. The H_2O masers

3.5.1. HC1

The new VLA radio maps from the WC observations were primarily made to see if there is any radio emission from the position of $\text{HC1} \equiv \text{MIR1}$ (which is outside the boundary of the maps published by WC). No radio continuum emission was found at the two wavelengths, with upper limits (5σ) of 3 and 10 mJy at 6 and 2 cm, respectively (see also Fig.7).

In Fig.8 a blown-up image of the HC1 source at K is shown. The new more accurate positions of the H_2O maser (WC) and the present better astrometry at K now show that the maser is located almost on top of the NIR source. This last one is clearly non-stellar due to a tail extending to the south-west. The point source in Fig.8 to the north-east of HC1 is a foreground star, since it is detected in all three bands and does not have a color excess, while that at the south-west end of the tail has been detected only in K, similarly to HC1 .

The observed color index (H - K) of HC1 is ≥ 4.7 , i.e. the largest of all the sources in the field. The flux density at K is 5 mJy. The expected 5 GHz emission, in the case that the K emission comes from free-free and free-bound emission of ionized gas, is 20 mJy, if we do not correct for reddening, and 135 mJy if we use $A_V = 23$, as for the neighboring UC HII region. In any case, the predicted flux is much larger the

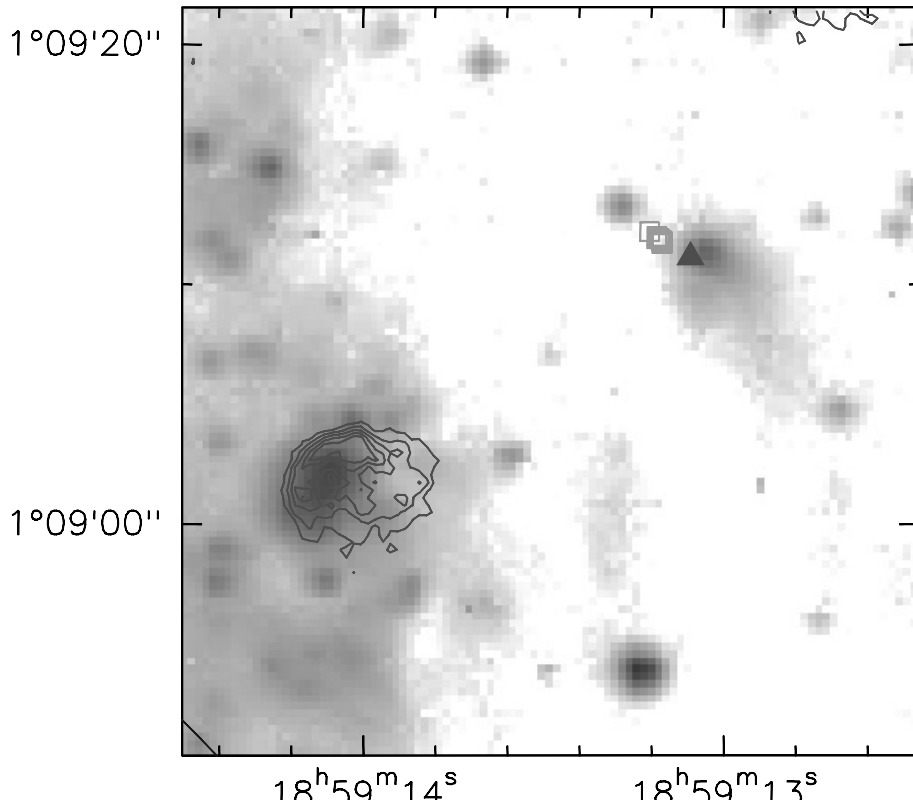


Fig. 7. Overlay of the 6 cm map (from the data of WC) with the K image. The filled triangle represents the position of the H₂O maser, while the open squares indicate the positions of the different components of the OH maser. Coordinates are at B1950.

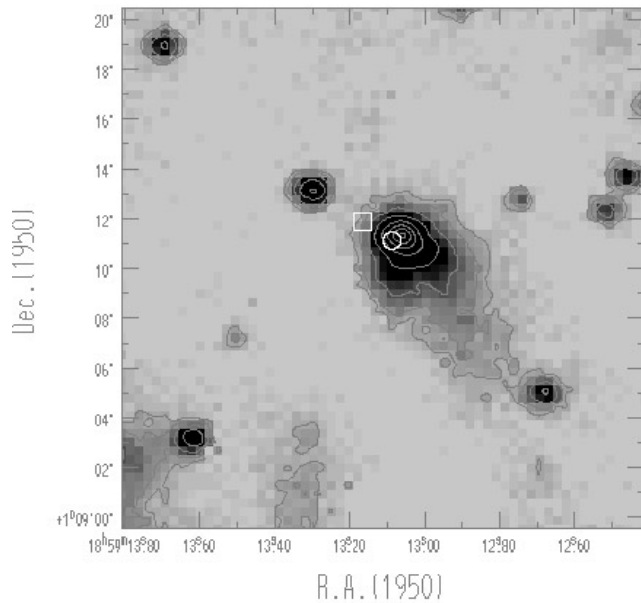


Fig. 8. K-contour map of a region surrounding the HC1 H₂O maser. An open circle represents the position of the water maser (Hofner & Churchwell 1996), while the OH maser position (Forster & Caswell 1986) is indicated with an open square.

the VLA upper limit. This does not automatically excludes that there could be an HII region, but implies that, if present, it is strongly self absorbed in the radio continuum.

In the following we shall consider the possibility that the K and 11.2 μm emissions come entirely from a hot dust envelope around a YSO.

The color temperature between K and 11.2 μm is 500 K, without correcting for reddening, or 610 K, if we correct the K emission for $A_V = 23$. A black-body that produces the observed flux densities should have a size of 9.7 - 7.3 AU and a luminosity of 240 - 300 L_\odot , in the two cases. Dust temperatures of several hundreds degrees can be reached only in the immediate surrounding of a YSO, at a radius consistent with the previous size. The implied luminosities could be produced by a pre-main sequence star inside a dust envelope, but could also be obtained by accretion during the protostellar phase, without requiring the presence of an already formed star; in fact Palla & Stahler (1993) predict accretion luminosities up to $10^3 L_\odot$ for mass accretions of $10^{-5} M_\odot/\text{year}$ and stellar masses between 2-6 M_\odot .

In summary, all the present evidences suggest that HC1 could be a YSO still in the accretion phase embedded in a hot dust envelope. The coincidence with the water maser confirms that the maser emission occurs in the earliest evolutionary phases of a YSO.

Other objects with characteristics similar to those of HC1 have already been found. The lack of a radio continuum counterpart associated with H₂O masers has been pointed out in many SFRs by Tofani et al. 1995. The prototype of this class of objects is the H₂O maser in W3OH (Turner & Welch 1984, Wink et al. 1994). An another example could be IRAS20126+4104

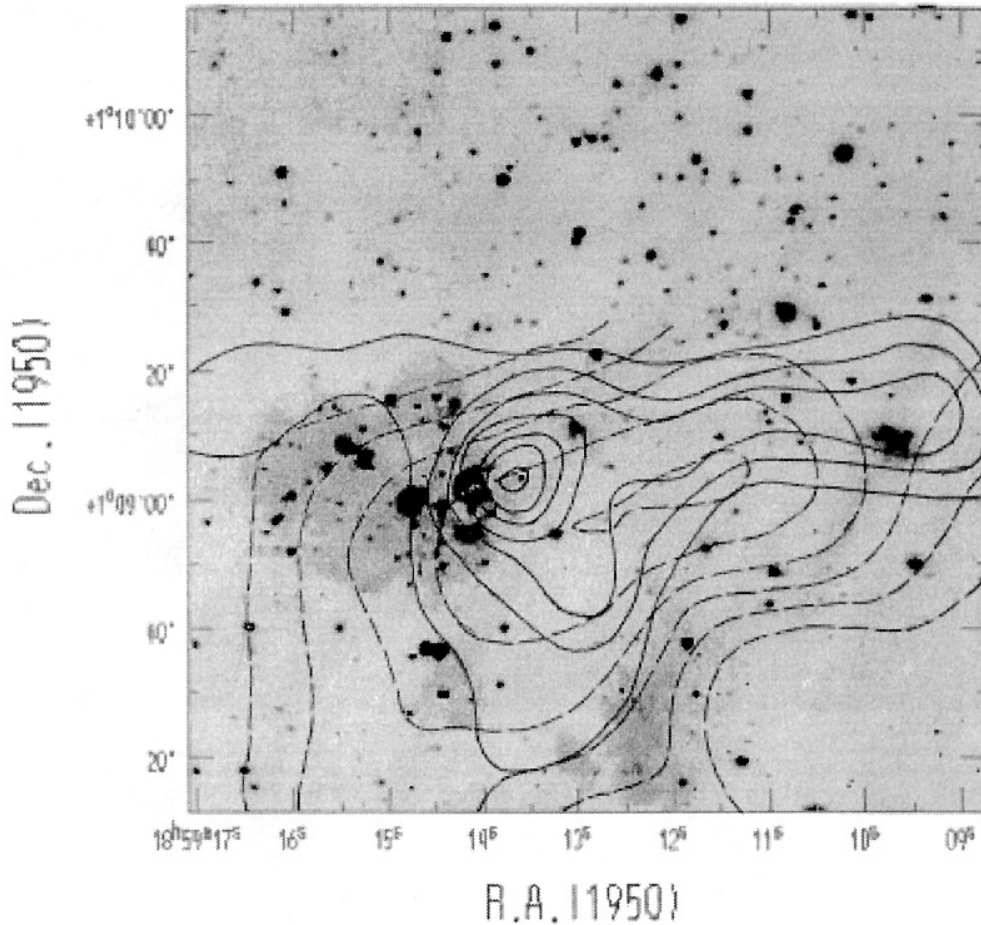


Fig. 9. 850 μm contour map (continuous line) (Jenness et al. 1995) and C^{18}O map (Vallée & MacLeod 1990) (dashed line) of G35.20-1.74 overlaid on the K image.

(Cesaroni et al. 1997) and component F in G9.62+0.19 (Hofner et al. 1996). In conclusion, as the resolution of the observation increases, there are more evidences that the maser emission occurs in the life of a YSO in phases preceding that of the UC HII region.

The distance of HC1 from the UC HII region (the projected value is 0.3 pc) seems to exclude any form of direct interaction between the two. Any agent traveling at the sound speed ($\sim 1 \text{ km s}^{-1}$) in the molecular cloud would take $3 \cdot 10^5$ years to cover that distance.

3.5.2. HC2

Not much can be said about this other maser. It is outside the field covered at $11.2 \mu\text{m}$ and also far from the field centre of the VLA observations. The closest NIR source (#1 in Table 1) is distant from the maser position by $2.6''$. It is detected in all three bands and its color indices show an IR excess, even though not as large as that of HC1. It is located within the western boundary of the molecular cloud/sub-mm source (see Fig.9).

3.6. Overall morphology of the G 35.20-1.74 SFR

The overall morphology of the SFR is shown in Fig.9, where the 850 μm map of Jenness et al. (1995) and the C^{18}O map of Vallée & MacLeod (1990) are overlaid on the K image.

The peak of the 850 μm emission is located between the UC HII region and HC1. With the present 850 μm resolution it is not clear if this is due to a true peak of cool dust emission between the two sources or, more simply, the sum of two independent contributions, one from the UC HII and one from HC1.

The diffuse HII region east of the UC one is outside both the 850 μm contours and the C^{18}O contours, indicating that dust and molecular gas have been destroyed by the radiation of the early type stars of the cluster.

The 850 μm and C^{18}O contours show a similar elongation in the east-west direction, and include the other maser HC2.

The morphology of the entire complex suggests that star formation has occurred independently in several places of the molecular cloud. The oldest event in time is that related to the stellar cluster and the diffuse HII region east of the molecular complex, the UC HII region may represent a younger event and the two masers the most recent ones.

4. Conclusions

Near and mid-infrared images obtained with sub-arcsec spatial resolution of the star forming complex G35.20-1.74 are presented. From our analysis of the infrared images, and from the comparison with similar resolution radio data, the main results are the following:

1) A young embedded stellar cluster has been detected from the near-IR images, on the east side of the cometary-shaped UC HII region. The cluster contains at least 21 members all within the boundary of the diffuse emission observed at 2.2 and 11.2 μm ($\sim 20''$ in radius). The majority of these members have infrared excesses and spectral types between B2-B3, assuming $A_V=23$.

2) Six sources have been found at 11.2 μm . The brightest of these (MIR3) has an extension of approximately $8''$, and coincides with the UC HII region. The sources MIR4,5, and 6 are located inside the cluster area. While the energy distribution of MIR4, and 5 indicates the presence of a circumstellar dust envelope around these sources, the infrared colors of MIR6 are consistent with the presence of a reddened early type star without IR excess.

3) At the position of the H₂O maser, distant about $20''$ from the UC HII, a very red source was found, detected only at 2.2 and 11.2 μm . At K the source (MIR1) shows a cometary-like morphology similar to that observed in several candidate protostars. In addition, the lack of the radio continuum and the very steep infrared spectrum indicate that MIR1 is an YSO in a very early phase. The association of this source with the H₂O maser confirms that water vapor masers can trace the youngest evolutionary stages of massive protostellar objects.

4) Finally, comparing the submillimeter and C¹⁸O maps with our infrared images, we can conclude that in G35.20-1.74 star formation has occurred independently (in time and space) in several places of the same large scale molecular clouds.

Acknowledgements. We thank E. Churchwell for providing us with the original VLA observations

References

- Andr  P., Montmerle T., 1994, ApJ 420, 837
 Anglada G., Estalella R., Pastor J., Rodriguez L.F., Haschick A.D. 1996, ApJ 463, 205
 Aspin C., Barsony M. 1994, A&A 288, 849
 Bridle A.H., Kesteven M.J.L. 1972, AJ 77, 207
 Cesaroni R., Churchwell E., Hofner P., Walmsley C.M., Kurtz S. 1994, A&A 288, 903
 Cesaroni R., Felli M., Testi L., Walmsley C.M., Olmi L. 1997 A&A in, press
 Churchwell E., Walmsley C.M., Cesaroni R. 1990, A&AS 83, 119
 Churchwell E., Walmsley C.M., Wood D.O.S. 1992, A&A 253, 541
 Codella C., Testi L., Cesaroni R. 1997, A&A submitted,
 Dyck H.M., Simon T. 1977, ApJ 211, 421
 Elias J.H., Frogel J.A., Matthews K., Neugebauer G. 1982, AJ 87, 1029
 Felli M. 1979 in "Stars and Star Systems", B. E. Westerlund ed, Reidel, 195
 Felli M., Testi L., Valdetaro R., Wang J.-J. 1997 A&A 320, 594
 Forster J.R., Caswell J.R. 1989, A&A 213, 339
 Genzel R., Downes D. 1977, A&AS 30, 145
 Hofner P., Kurtz S., Churchwell E., Walmsley C.M., Cesaroni R., 1996 ApJ 460, 359
 Hofner P., Churchwell E., 1996 A&AS 120, 283
 Howard E.M., Pipher J.L., Forrest W.J. 1994 ApJ 425, 707
 Hunter T.R., Testi L., Taylor G.B. et al. 1995 A&A 302, 249

- Jenness T., Scott P.F., Padman R. 1995, MNRAS 276, 1024
 Lada C.J. 1987, IAU symposium 115, *Star Forming Regions*, eds. M. Peimbert & J. Jugaku, Kluwer, Dordrecht
 Lada C.J., DePoy D.L., Merrill K.M., Gatley I. 1991, ApJ 374, 533
 Lagage P.O., Jouan R., Masse P., Mestreau P., Tarrus A. 1992, in 42d ESO Conf. "Progress in Telescope and Instrument", ed.M.H.Hulrich (Munche:ESO), p.601
 Moorwood A.F.M., Salinari P. 1981 A&A 94, 299
 Natta A., Panagia N. 1976 A&A 50, 191
 Onello J.S., Phillips J.A., Benaglia P., et al. 1994 ApJ 426, 249
 Palla F., Stahler S.W. 1993 ApJ 418, 414
 Palla F., Testi L., Hunter T.R. et al. 1995 A&A 293, 521
 Panagia N. 1973 AJ 78, 929
 Persi P., Roth M., Tapia M., Ferrari-Toniolo M., Marenzi A.R. 1994, A&A 282, 474
 Persi P., Roth M. Tapia M. et al. 1996 A&A 307, 591
 Persson S.E., West S.C., Carre D.M., Sivaramakrishnan A., Morphey D.C. 1992, PASP 104, 204
 Stetson P.B. 1987 PASP 99, 101
 Testi L., Felli M., Persi P., Roth M. 1994, A&A 288, 634
 Tofani G., Felli M., Taylor G.B., Hunter T.R. 1995. A&AS 112, 299
 Turner J.L., Welch W.J. 1984, ApJ 287, L81
 Turner T.E. 1979, A&AS 37, 1
 Vall e J.P., MacLeod J.M. 1990, ApJ 358, 183
 Wink J.E., Duvert G., Guilloteau S. et al. 1994, A&A 281, 505
 Wood D.O.S., Churchwell E. 1989, ApJS 69, 831
 Woodward C.E., Helfer H.L., Pipher J.L. 1985 A&A 147, 84
 Zeilik M.II., Lada C.J., 1978, ApJ 222, 896